

UNIVERSITY OF TRENTO



Department of Industrial Engineering
Master degree in Mechatronics Engineering
Dynamics of Vehicles

Assignment 1: tyre fitting

Team 6

Professor:

Prof. Biral Francesco

Students:

*Consalvi Natale
Pettene Mattia
Zumerle Matteo*

ACADEMIC YEAR 2022/23

Contents

| | | |
|-------------------|---|-----------|
| 1 | Introduction | 1 |
| 1.1 | Model, geometry and sign convention | 1 |
| 1.2 | General fitting procedure | 1 |
| 1.2.1 | Data cropping | 2 |
| 1.2.2 | Set of conditions for each analysis | 2 |
| 1.2.3 | Optimization of residuals | 2 |
| 1.2.4 | Variations of guess vector and parameter boundaries | 2 |
| 1.2.5 | Model validation | 3 |
| 1.2.6 | Tire coefficients backup | 3 |
| 1.3 | Delivered files description | 3 |
| 2 | Results | 4 |
| 2.1 | Pure longitudinal force | 4 |
| 2.1.1 | Reference conditions | 4 |
| 2.1.2 | Vertical load variation | 5 |
| 2.1.3 | Longitudinal cornering stiffness | 6 |
| 2.1.4 | Camber angle variation | 7 |
| 2.2 | Pure lateral force | 7 |
| 2.2.1 | Reference condition | 8 |
| 2.2.2 | Vertical load variation | 8 |
| 2.2.3 | Lateral cornering stiffness | 9 |
| 2.2.4 | Camber angle variation | 10 |
| 2.3 | Pure aligning moment | 10 |
| 2.3.1 | Reference condition | 11 |
| 2.3.2 | Vertical load variation | 11 |
| 2.3.3 | Camber angle variation | 12 |
| 2.4 | Combined longitudinal force | 14 |
| 2.4.1 | Reference condition | 14 |
| 2.5 | Combined lateral force | 15 |
| 3 | Result discussion | 18 |
| 3.1 | Cornering stiffness focus | 18 |
| 3.2 | Variable load on the pure lateral stiffness focus | 19 |
| 4 | Conclusion | 21 |
| References | | 22 |

1 Introduction

1.1 Model, geometry and sign convention

The first essential point from which describe vehicle dynamics is how tires generate forces and moments in contact with the road surface. Tyres are the only elements able to generate the longitudinal force to accelerate and brake and at the same time can generate the lateral forces to steer the vehicle. The formulation used follows a semi-empirical model in which the action is described using fitting of experimental data. To do that it is used the **Pacejka 1996** semi-empirical tyre model based on the **Magic Formula**.

Pacejka model permits to handle with tires in steady state behavior that naturally shows the presence of longitudinal tyre force F_x , lateral tyre force F_y and self aligning moment M_z according to the commands given to the car. The tyre response in terms of forces and moments is highly affected by visco-elastic capacity that activate energy dissipation processes and hysteresis mechanisms, but also from its camber angle γ .

All the following studies will be based on two different tyre data-set done on the same pneumatic model: **Hoosier 6.0 / 18.0 - 10 LCO** and the **adapted SAE** sign convention, in order to use Pacejka formulation.

Pacejka's magic formula is essential to fit into an analytic function all the curves composed by experimental data, in order to generate a performance map of the tyre model in different operating condition, in particular changing the nominal vertical load applied and the camber angle. Its general form is the following:

$$\begin{aligned}y(x) &= D \sin(C \arctan(Bx - E(\arctan(Bx)))) \\Y(X) &= y(x) + S_V \\x &= X + S_H\end{aligned}$$

in which X represent the input variable that can be the practical slip κ or the slip angle α , while Y is the output corresponding formula, so F_X or F_Y or M_Z .

B parameter works as stiffness factor, C is the shape factor, D the peak value, E is the curvature factor, and at the end S_H and S_V are horizontal and vertical shifts. A note about the value BCD that is the slope at the origin ($x = y = 0$).

The approach is the method of *similarity*, which shows that the slip curves remain similar even when the operating condition is changed from the reference condition, consisting of zero camber angle ($\gamma = 0$), free rolling condition ($\kappa = 0$) or zero slip angle ($\alpha = 0$) and with the nominal vertical load applied (F_{Z0}).

1.2 General fitting procedure

Two dataset were provided to study the possible behaviors of the tyre: **B1464run30.mat** for the study of pure longitudinal force and combined behavior, and **B1464run23.mat** for that of pure lateral and aligning moment.

The first step was the modification of the **Maple** file to generate the functions that will be stored in the **tyre_lib** root, which will be useful for calculating coefficients, forces and

moments by exploiting implementations of the Magic Formula. These will be used in the `main_tire_data_analysys.m` file to streamline the calculation process.

A note on the generated functions: team started looking at the pure longitudinal provided functions and generate the pure lateral, combined longitudinal and lateral, aligning moment ones, both for calculate the coefficient and forces/torques. The team also modified the outputs of the functions so that they could generate the coefficients needed for the calculations implemented in the main in MATLAB.

1.2.1 Data cropping

The data are initially cropped in the interval in which the pressure is higher: this can guarantee a more stable tyre behavior. The selected dataset portion is the one between the following sample for the pure longitudinal case:

$$cut_start = 19028 \quad cut_end = 37643 \quad (1)$$

While for the lateral force analysis, the samples interval is:

$$cut_start_pl = 31350 \quad cut_end_pl = 54500 \quad (2)$$

The entire dataset is composed by the imposed longitudinal slip κ , side slip angle α , vertical load F_z and camber angle γ and also by the measured longitudinal force F_X , lateral force F_Y and aligning moment M_Z . These data are divided into tables, using the values imposed during the tests, contained in the Excel file **1464 Summary Tables**. This procedure has been done for γ , F_z and α values.

1.2.2 Set of conditions for each analysis

Using the function `intersect_table_data`, it is possible to generate a table structure that contains all the values of the dataset that satisfy some conditions. In general, the Magic Formula coefficients are derived by proceeding, for each type of force, with three analyses: pure condition, vertical load variation, and camber variation. For example, to analyze the pure condition, it is necessary to select the particular range in which the imposed vertical load F_z is equal to the nominal one F_{z0} , the camber angle is equal to 0, and, depending on the analysis performed, the longitudinal or side slip is zero.

1.2.3 Optimization of residuals

For each analysis, after selecting the range in which it is conducted, the parameters that influence that particular characteristic of the curve are selected. Then a first guess vector is created and it is one of the input of the MATLAB function, called `fmincon`. This function is able to minimize the residuals by modifying the parameters and creating a new optimized parameter vector that it will be used to plot the fitted curve.

1.2.4 Variations of guess vector and parameter boundaries

After optimizing the parameters, they are placed inside a struct that will contain all the coefficients, previously initialized. For each test, under pure conditions, varying vertical load, and varying camber, curves, that fit the specific dataset, are plotted. Looking at the graphs, it was possible to modify the required parameters by applying boundaries to them.

1.2.5 Model validation

To see if the results obtained were consistent, two approaches were used:

- observe the R^2 index of the residuals;
- calculate the Magic Formula coefficients.

R^2 is the coefficient of determination and is calculated for each optimization, with values between 0 and 1, which, if close to 1, indicate that the model is able to fit the tyre dataset well. It is defined as follow:

$$R^2 = 1 - fval \quad (3)$$

where $fval$ is the value of the residuals calculated with the optimal parameters inside the function `fmincon`.

The second approach, carried out after optimizing all parameters related to a given force or moment, was to calculate the magic formula coefficients, particularly those that had to meet certain conditions dictated by theory. In particular, the following results were checked:

| F_{x0} | F_{y0} | M_{z0} | F_x | F_y |
|--------------|--------------|--------------|--------------|--------------|
| $C_x > 0$ | $C_y > 0$ | $C_t > 0$ | $G_{xa} > 0$ | $G_{yk} > 0$ |
| $D_x > 0$ | $\mu_y > 0$ | $B_t > 0$ | $B_{xa} > 0$ | $B_{yk} > 0$ |
| $E_x \leq 1$ | $E_y \leq 1$ | $E_t \leq 1$ | | |

An important focus was reserved for stiffness; in fact, these played a very important role in the analysis, in particular K_{yk} , which will be especially explored in chapter 3.1.

1.2.6 Tire coefficients backup

The results are saved and stored in a unique struct inside `tyre_coeffs_team6.mat` file. This file is attached with this report and permits at anytime to look at the parameters results founded without running the entire code again.

1.3 Delivered files description

As mentioned earlier, in the delivered folder is the main `main_tyre_data_analysis.m`, which can calculate the coefficients and produce all the graphs in the report. The latter uses the functions that were generated from `TyreModel-MF96.mw` and are contained within the `tire_lib` folder. The datasets are contained in the folder of the same name.

A more accurate description can be viewed within the GitHub repository, in the `README.md` file: <https://github.com/mattiapettene/DoV-Project-team6>.

2 Results

In this chapter will be presented the results that the team achieved. To obtain them, the procedure described in Section 1.2 is used. The outcomes are calculated as follows: for each force and moment, except for combined longitudinal force F_X , three different procedures are done: in pure conditions, with a vertical load variation and with a change in camber angle. In a first comments, the conditions under which the fitting procedure takes place are described. Then, within a table, the parameters are listed and the guess, the lower and upper bound are reported for each. Using these, it is possible to calculate the optimal values, which are reported. The last row of the table shows the R^2 index, ranging from 0 to 1. To enable better understanding, the graph showing the comparison between the experimental data and the obtained functions is also shown. A comment is included to conclude the analysis, in which critical issues encountered during the analysis are notified, if any.

It is important to note the presence of " \sim " within boundaries: these indicate that no bound has been imposed on the parameter in question.

2.1 Pure longitudinal force

In order to predict the behaviour of the pure longitudinal force F_{X0} , it is assumed that the vehicle has only a not lateral behavior: the car moves on a straight line, without any steering wheel angle: indeed, as is possible to see from cropped data, the side slip angle α is null at anytime.

2.1.1 Reference conditions

The first analysis is done in nominal conditions: side slip angle $\alpha = 0^\circ$, camber angle $\gamma = 0^\circ$ and vertical load $F_{Z0} = 220N$, in order to find the pure longitudinal force F_{X0} in function of the longitudinal slip κ . Then the following set of guess and bounds is imposed, it is essential to compute the optimization. Then the parameters are used to compute the Magic Formula coefficients, in order to get the correct longitudinal force graph.

| | pCx1 | pDx1 | pEx1 | pEx4 | pHx1 | pKx1 | pVx1 |
|----------------------|---------------|-------|----------|----------|-----------|---------|-----------|
| Guess | 1 | 2 | 1 | 0 | 0 | 1 | 0 |
| L bound | 1 | 0.1 | 0 | 0 | -10 | 0 | -10 |
| U bound | 2 | 4 | 1 | 1 | 10 | \sim | 10 |
| Optm par | 1.539 | 3.147 | 1.133e-2 | 8.063e-2 | -2.092e-5 | 8.241e1 | -8.577e-2 |
| R² | 0.9955 | | | | | | |

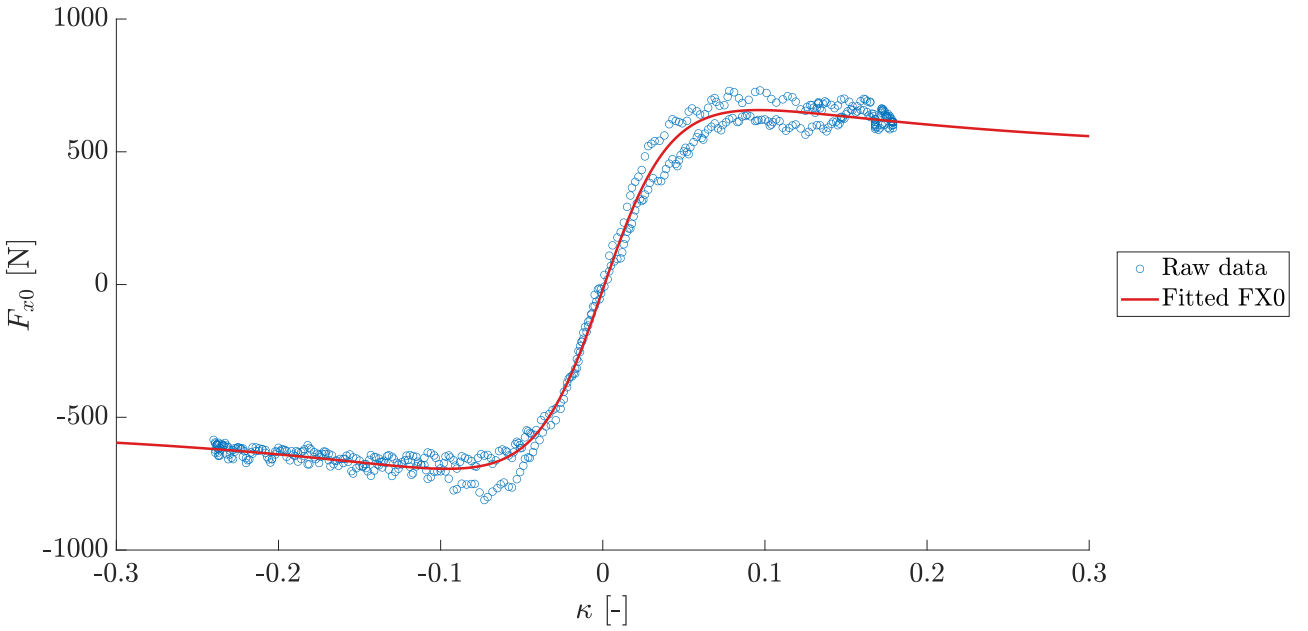


Figure 1: Comparison between the fitted curve on the raw data for the pure longitudinal force F_{X0} in reference conditions.

2.1.2 Vertical load variation

In this case, the null side slip angle condition remains and also the camber angle one. Thanks to the table interpolation function, only the vertical load F_Z is left free. During the test, the imposed values of F_Z are $220N$, $700N$, $900N$, $1120N$, that are collected with a tolerance of $100N$. Higher the vertical load, higher the value that the curves reach, ceiling.

| | pDx2 | pEx2 | pEx3 | pHx2 | pKx2 | pKx3 | pVx2 |
|----------------------|---------------|-----------|----------|----------|-----------|----------|-----------|
| Guess | 0 | 0 | 0 | 0 | 0 | 0 | 0 |
| L bound | ~ | ~ | ~ | ~ | ~ | ~ | ~ |
| U bound | ~ | ~ | ~ | ~ | ~ | ~ | ~ |
| Optm par | -2.496e-1 | -3.619e-1 | 1.059e-1 | 1.050e-3 | -1.859e-3 | 1.536e-1 | -2.559e-2 |
| R² | 0.9971 | | | | | | |

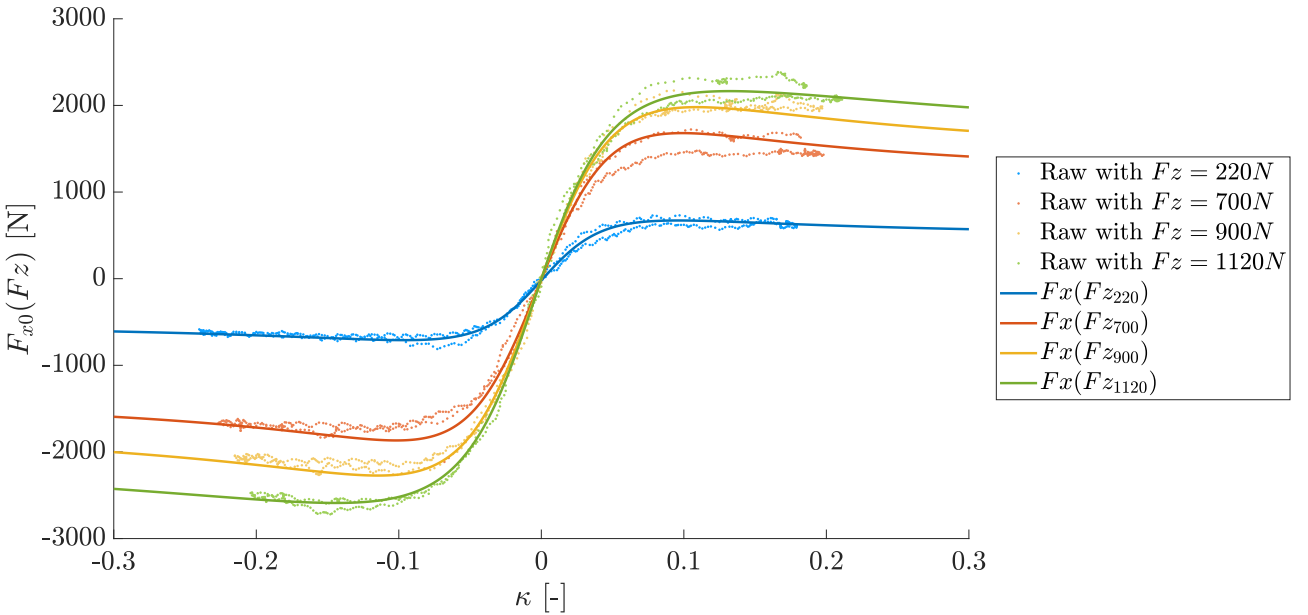


Figure 2: Fitted curves on the raw data for the pure longitudinal force F_{X0} varying the vertical load F_Z .

2.1.3 Longitudinal cornering stiffness

The longitudinal cornering stiffness K_{xk} is computed using the definition and it is shown with two different points of view, as a function of the vertical load applied F_Z and as a function of the longitudinal slip κ .

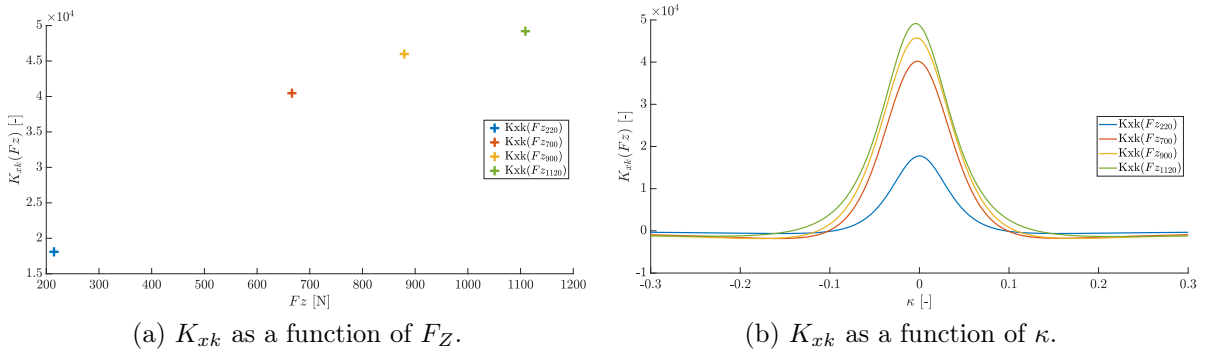


Figure 3: Longidutudinal cornering stiffness K_{xk} when the vertical load F_Z changes.

This value is an index of the inclination of the curves at zero longitudinal slip. Its value tends to increase, increasing the vertical load applied until reaching a saturation value, as shown in figure 3a.

Then it is presented the map that shows the behavior of K_{xk} as function of the longitudinal slip κ . As is possible to notice from picture 3a, higher the vertical load, higher will be the pick of the curve, consistently with figure 3a.

Note that is possible to go back to figure 3a, drawing a straight vertical line passing through the origin, in $\kappa = 0$. The originated intersection will correspond to the points of the figure 3a. For sake of clarity, the color map has been maintained.

2.1.4 Camber angle variation

Starting from the fact that the influence of camber on the longitudinal force is assumed not to occur [1], it has done a study to prove that.

A similar procedure made for the previous load variation has been done also regarding the camber angle, this time keeping at constant value both the load and the side slip angle, respectively equal to $F_{Z0} = 220N$ and $\alpha = 0^\circ$. The variation has been computed on the camber angle of the wheel, looking for the behavior generated for 0° , 2° , 4° values, with a tolerance of 0.5° . In this case there was only a singular parameter to be optimized and it is:

| pDx3 | |
|----------------------|---------------|
| Guess | 0 |
| L bound | ~ |
| U bound | ~ |
| Optm par | 1.844e1 |
| R² | 0.9938 |

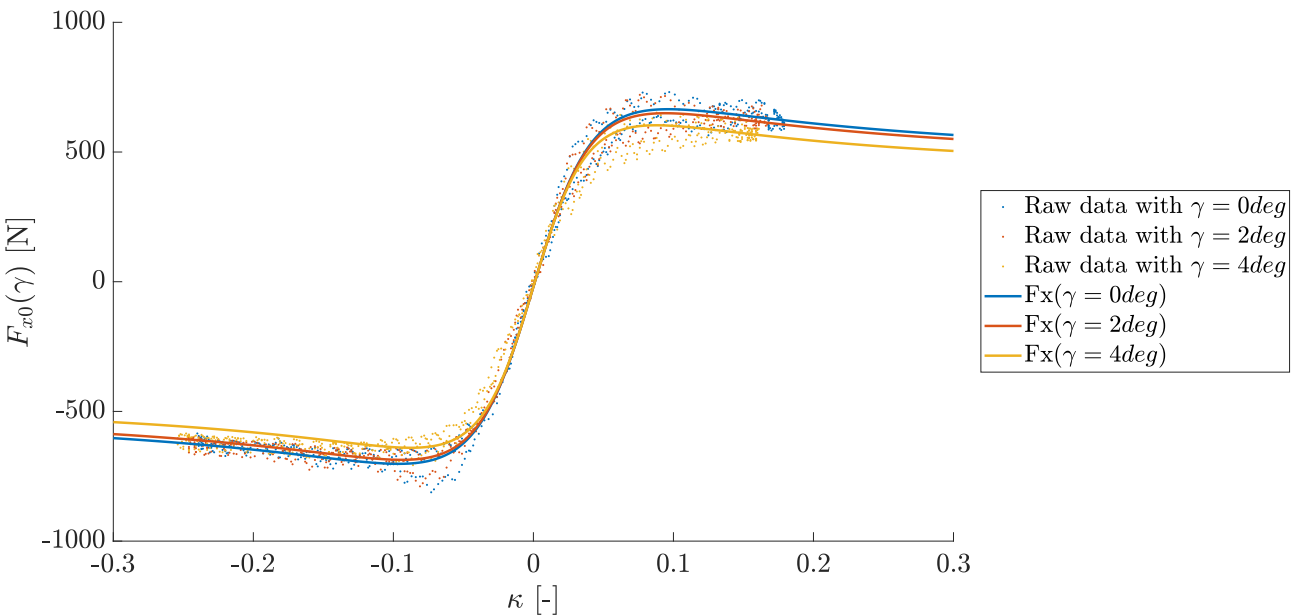


Figure 4: Fitted curve on the raw data for the pure longitudinal force F_{X0} varying the camber angle γ of the tyre.

2.2 Pure lateral force

The same study procedures are also computed for the pure lateral force analysis: in this chapter will be seen the particular case when the dynamic of the tyre is characterized by a lateral force presence, without any additional longitudinal component, so $\kappa = 0$. Although the behavior is different, the procedure is very similar to that seen in section 2.1: the team has optimize the parameters that affect F_{Y0} under pure conditions, under load variation, and under camber angle variation. Additionally an important focus is reserved for the lateral cornering stiffness K_{ya} .

2.2.1 Reference condition

The nominal curve is founded out putting at a longitudinal slip $\kappa = 0$, a camber angle $\gamma = 0^\circ$ and a vertical load of $Fz = 220N$, in order to find the lateral force F_{Y0} as a function of the lateral slip angle α .

| | pCy1 | pDy1 | pEy1 | pHy1 | pKy1 | pKy2 | pVy1 |
|----------------------|---------------|-------|--------|----------|---------|-------|-----------|
| Guess | 1.3 | 2.7 | -1 | 0.0038 | 170 | 5.05 | -0.0792 |
| L bound | 1.1 | 2.5 | ~ | ~ | 0 | 4.9 | ~ |
| U bound | ~ | ~ | 1 | ~ | 175 | 5.1 | ~ |
| Optm par | 1.135 | 2.717 | 0.4583 | 3.803e-2 | 1.675e2 | 4.981 | -7.923e-2 |
| R² | 0.9963 | | | | | | |

The fitted curve, shown in figure 5, presents a good fitting behavior, as is possible to verify from the R^2 value present in the table.

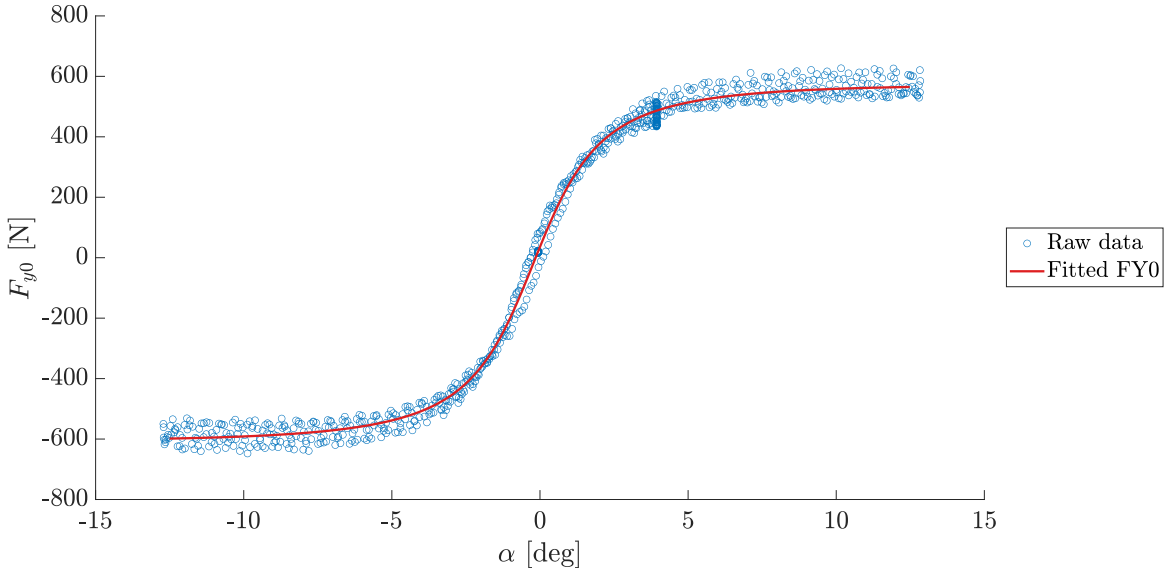


Figure 5: Fitted curve on the raw data for the pure lateral force F_{Y0} in pure conditions.

2.2.2 Vertical load variation

In this case the table interpolation has been done looking at the intersection of the data when the longitudinal slip is $\kappa = 0$ and the camber angle is $\gamma = 0^\circ$. The vertical load is left free to change.

| | pDy2 | pEy2 | pHy2 | pVy2 |
|----------------------|---------------|----------|----------|----------|
| Guess | -0.05 | -1 | 0 | 0 |
| L bound | -0.2 | ~ | ~ | ~ |
| U bound | 0 | ~ | ~ | ~ |
| Optm par | -8.464e-2 | 7.214e-2 | 1.004e-5 | 7.942e-3 |
| R² | 0.9912 | | | |

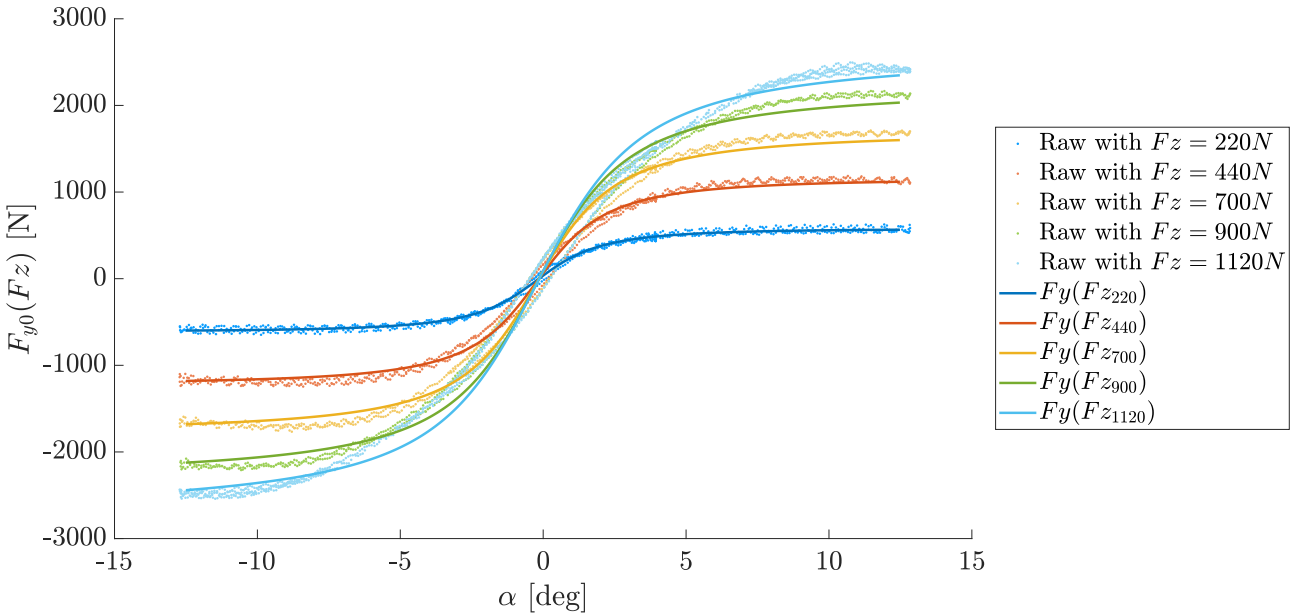


Figure 6: Fitted curve on the raw data for the pure lateral force F_{Y0} in the case of vertical load variation.

The fitting result is good in the center and tails of the curves, while for small positive and negative values of side slip angles there is a conspicuous detachment from the measured data and the curve. Even if this conduct, the R^2 value tell that the fitted curve has been done in any case in a good way. This behavior is given by the presence of stringent boundaries, the latter of which were imposed to obtain cornering stiffness trends consistent with the theoretical trends described in section 1.

2.2.3 Lateral cornering stiffness

Also for the pure lateral case is possible to calculate the lateral cornering stiffness: K_{ya} . Also in this case it is represented as a function of the imposed vertical load F_Z and of the side slip angle α .

This value shows the inclination of the lateral force curves at zero value of lateral slip angle α . Its value tends to increase, increasing the vertical load applied until reaching a saturation value. This behavior is shown in figure 7.

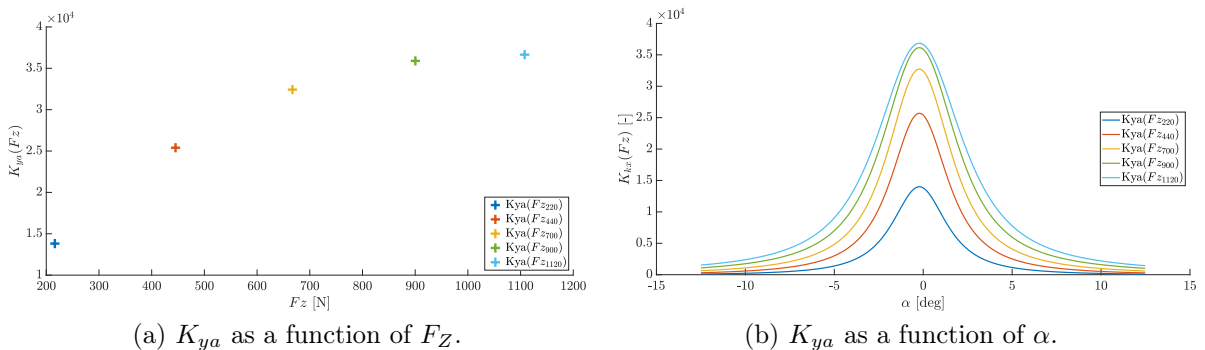


Figure 7: Lateral cornering stiffness K_{ya} when the vertical load F_Z changes.

Concerning this topic, a specific study has been done and it has been collected and explained in *Result discussion* section.

2.2.4 Camber angle variation

In this section, as shown in figure 8, is done the interpolation of all the data that shares a side zero slip angle $\alpha = 0^\circ$, a fixed vertical nominal force $F_{Z0} = 220N$, letting free to change the camber angle γ . The imposed values are from 0 to 4 [deg], with unitary steps changes.

| | pDy3 | pEy3 | pEy4 | pHy3 | pKy3 | pVy3 | pVy4 |
|----------------------|---------------|-----------|--------|-----------|----------|-------|------|
| Guess | -2 | 0 | -2 | 0 | 0 | 0.15 | 0 |
| L bound | ~ | ~ | -3 | ~ | ~ | ~ | ~ |
| U bound | ~ | ~ | ~ | ~ | ~ | ~ | ~ |
| Optm par | -1.089e-1 | -9.200e-3 | -2.945 | -1.402e-4 | 7.433e-2 | 1.027 | 0 |
| R² | 0.9960 | | | | | | |

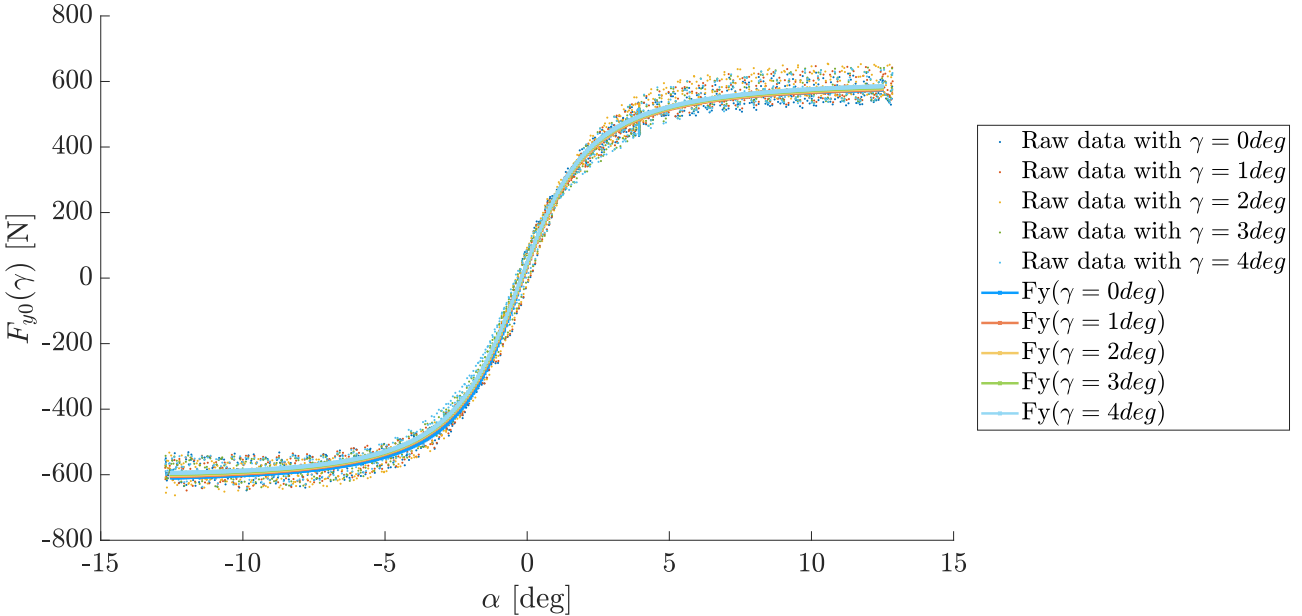


Figure 8: Fitted curve on the raw data for the pure lateral force F_{Y0} changing the camber angle of the tyre.

The result obtained shows a really serrated series of curves that are difficult to distinguish one from another also due to the fact that in some points (especially in the central region) all tends to overlap.

This behavior could have been caused by a bad data collection that sees the different values collected in a oscillating way with a mean curve that is similar for all the degrees showed.

2.3 Pure aligning moment

This aligning moment is calculated in the case of the only pure lateral force presence due to the fact that the one generate from the combined behavior becomes too much complex and elaborated to be faced on this study.

Due to the derivation from the pure lateral force, a part of the all aligning moment parameters used come from the previous parameters force ones. In fact it has been necessary to include them in the `MF96_MZ0_coeffs.m` function precisely, with an internal call to the already generated `MF96_FY0_coeffs.m` due to the need of the By , Cy , SVy , Kya , SHy parameters.

2.3.1 Reference condition

The nominal curve is founded blocking all the degrees of freedom to the nominal values and optimizing the nine parameters. This computation has been the one that required more resources in terms of time due to the high number of values to compute. Now follows the table containing guess, boundaries, optimal and R^2 values. Then, in figure 9, is showed the final fitting result.

| | qBz1 | qBz9 | qBz10 | qCz1 | qDz1 | qDz6 | qEz1 | qEz4 | qHz1 |
|----------------------|---------------|----------|-----------|-------|----------|----------|-----------|-----------|----------|
| Guess | 6 | 0 | 0.7 | 1 | 0 | 0 | -1 | -0.5 | 0 |
| L bound | -10 | -1 | -5 | -5 | -10 | -10 | -0.8 | -0.8 | -1 |
| U bound | 10 | 1 | 5 | 5 | 10 | 10 | 0.8 | 0.8 | 1 |
| Optm par | 1.848 | 2.686e-3 | -3.459e-1 | 4.999 | 5.898e-2 | 1.205e-2 | -7.998e-1 | -3.561e-1 | 1.008e-2 |
| R² | 0.3711 | | | | | | | | |

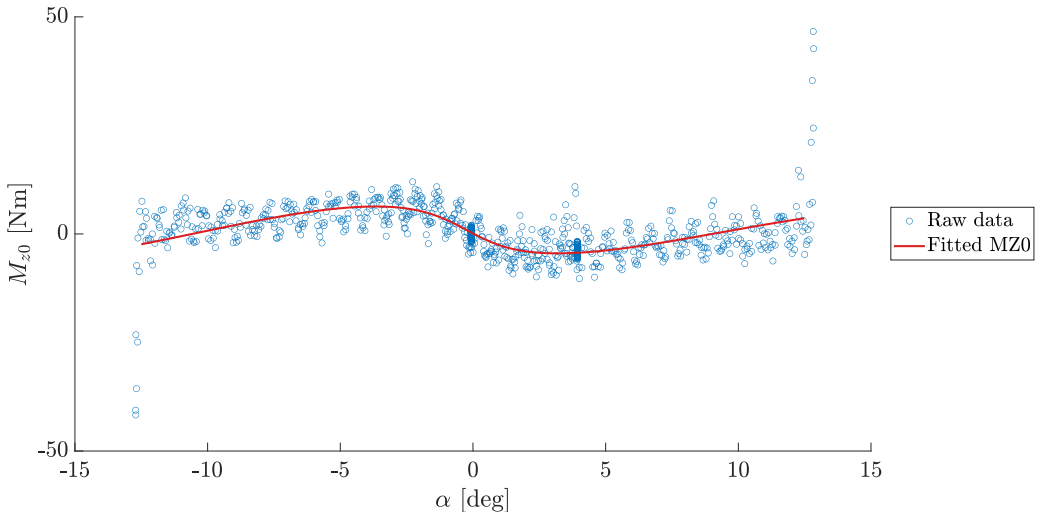


Figure 9: Fitted curve on the raw data for the pure aligning moment in nominal conditions.

As is possible to see from a especially low R^2 value, the goodness of fitting is not particularly high: from the picture this is not verified, with a well modelled curve all seems to be good. Probably this behavior is due to the presence of the two exploding tails that could generate a higher difference between the fitted curve and the real data measured. This can influence negatively the R^2 value, making it decrease.

2.3.2 Vertical load variation

In this section it has been studied the intersection of the data when the camber angle is $\gamma = 0[\text{deg}]$: the vertical load is left free to change. Corresponding guess, boundaries optimum and R^2 values are here reported.

| | qBz2 | qBz3 | qDz2 | qDz7 | qEz2 | qEz3 | qHz2 |
|----------------------|---------------|-----------|-----------|-----------|-------|-----------|------------|
| Guess | 0 | 0 | 0 | 0 | 0 | 0 | 0 |
| L bound | -4 | -4 | -5 | -5 | -2 | -1 | -5 |
| U bound | 4 | 4 | 5 | 5 | 2 | 1 | 5 |
| Optm par | -3.673e-2 | -1.591e-2 | -6.105e-3 | -3.992e-3 | 1.999 | -4.196e-1 | -1.3408e-4 |
| R² | 0.9574 | | | | | | |

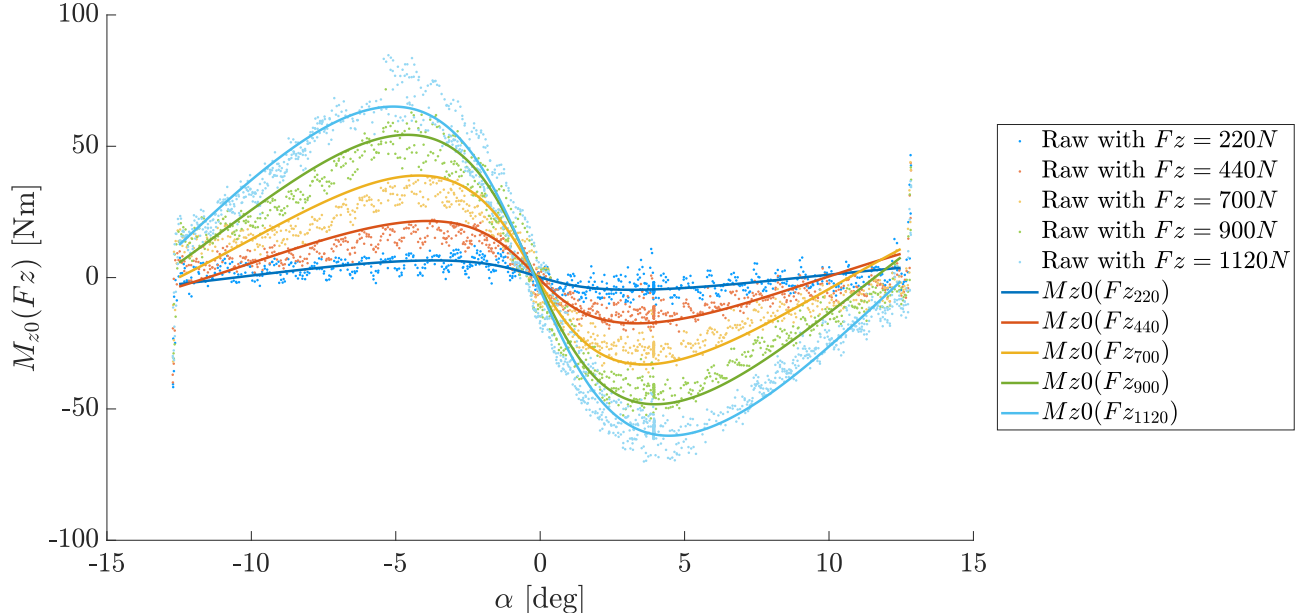


Figure 10: Fitted curve on the raw data for the pure aligning moment varying the vertical load applied.

Fitting of figure 10 can be considered good for all curves except for the green and blue ones that are not able to reach perfectly the pick values, remaining a little below these. Anyhow, as told by the R^2 value, the result is acceptable.

2.3.3 Camber angle variation

Last point analyzed for the pure aligning moment study regards the variation effects on camber angle. The intersection table has made taking fixed only the vertical load value at its nominal value. Hypothesis starting point for the minimizer, limits and optimum result presented in the table.

| | qBz4 | qBz5 | qDz3 | qDz4 | qEz5 | qDz8 | qDz9 | qHz3 | qHz4 |
|----------------------|---------------|-----------|-------|----------|---------|-------|------|-----------|------|
| Guess | 0 | 0 | 0 | -1 | 0 | 0.6 | 0.2 | 0 | 0 |
| L bound | ~ | ~ | -3 | ~ | ~ | ~ | ~ | ~ | ~ |
| U bound | ~ | ~ | -3 | ~ | ~ | ~ | ~ | ~ | ~ |
| Optm par | 9.671e-1 | -4.208e-2 | 1.707 | -1.620e1 | 5.258e1 | 1.369 | 2e-1 | -5.978e-1 | 0 |
| R² | 0.4633 | | | | | | | | |

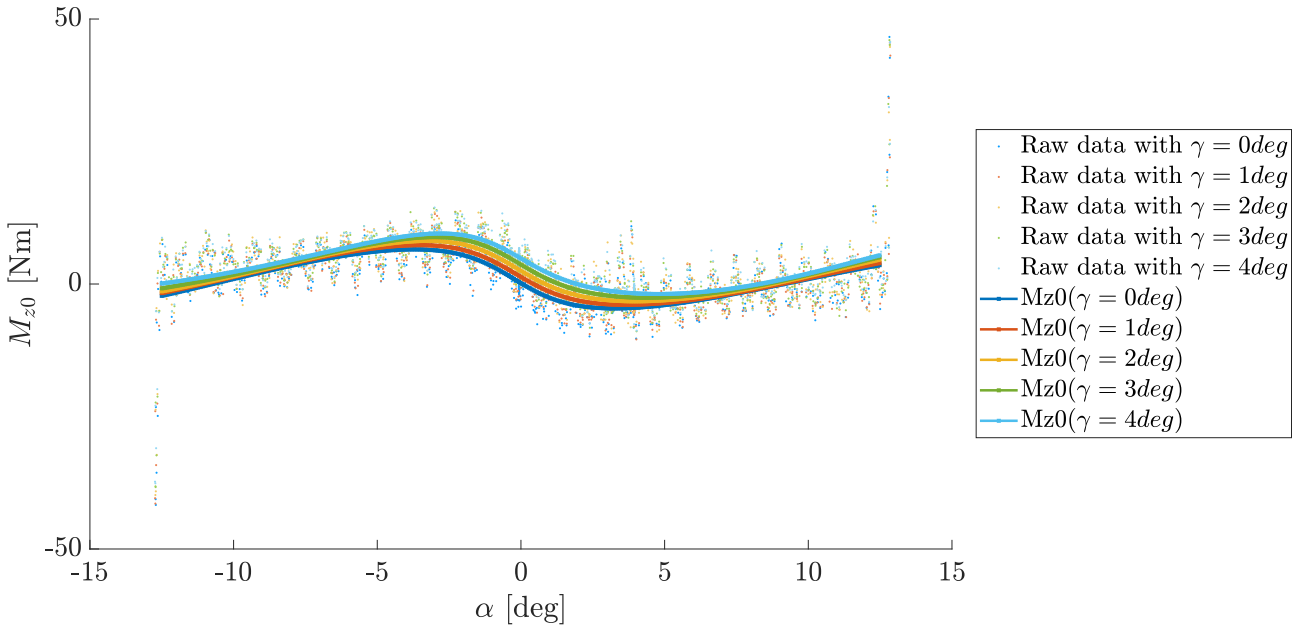


Figure 11: Fitted curve on the raw data for the pure aligning moment varying the camber angle.

Fitted result shows, for central values a open disposition of the curve, where is clear the disposition order, which sees an increasing of the output moment, increasing the camber angle. Going towards the tails all the curves overlap each other with a no more clear behavior that distinguish one from another. Regarding the R^2 , the value is not as good as the camber angle variation sees in the pure lateral force behavior. The low value is most likely due to the high variation with which data are collected during the experiment: it is simple to recognise a clear oscillation path of the data points. Due to the average value is in the middle, fitted curve will settle down on the average, letting a huge distance between fitted and real point. Then also the exploding tails do not help to reduce the R^2 value. It is the same behavior found and discussed in 2.2.4 and 2.3.1 paragraphs.

2.4 Combined longitudinal force

Unlike previous cases, in this analysis the team is interested on the presence of both components of the slip vector: longitudinal and lateral. In fact, the complete dataset is considered and, since the latter has a continuous variation of longitudinal slip, the combined behavior is analyzed as a function of κ for different steps of lateral slip angle α .

2.4.1 Reference condition

The longitudinal force, in combined case, is analysed with three different values of side slip angle, 0° , 3° and 6° . In this case the table, obtained thanks to the intersection of different ranges of the dataset, represents the condition in which the vertical load is equal to $F_{Z0} = 220N$ and the camber angle is null. In this section the combined behaviour is analysed in this reference condition, due to the fact that the variations of vertical load and camber angle are included inside the pure expression of the force.

| | rBx1 | rBx2 | rCx1 | rHx1 |
|----------------|---------------|----------|-------|-----------|
| Guess | 17 | -11 | 1 | 0 |
| L bound | 0 | -16.5 | -0.5 | -0.015 |
| U bound | 20 | 20 | 10 | 0.015 |
| Optm par | 1.997e1 | -1.578e1 | 1.228 | -8.222e-3 |
| R ² | 0.9947 | | | |

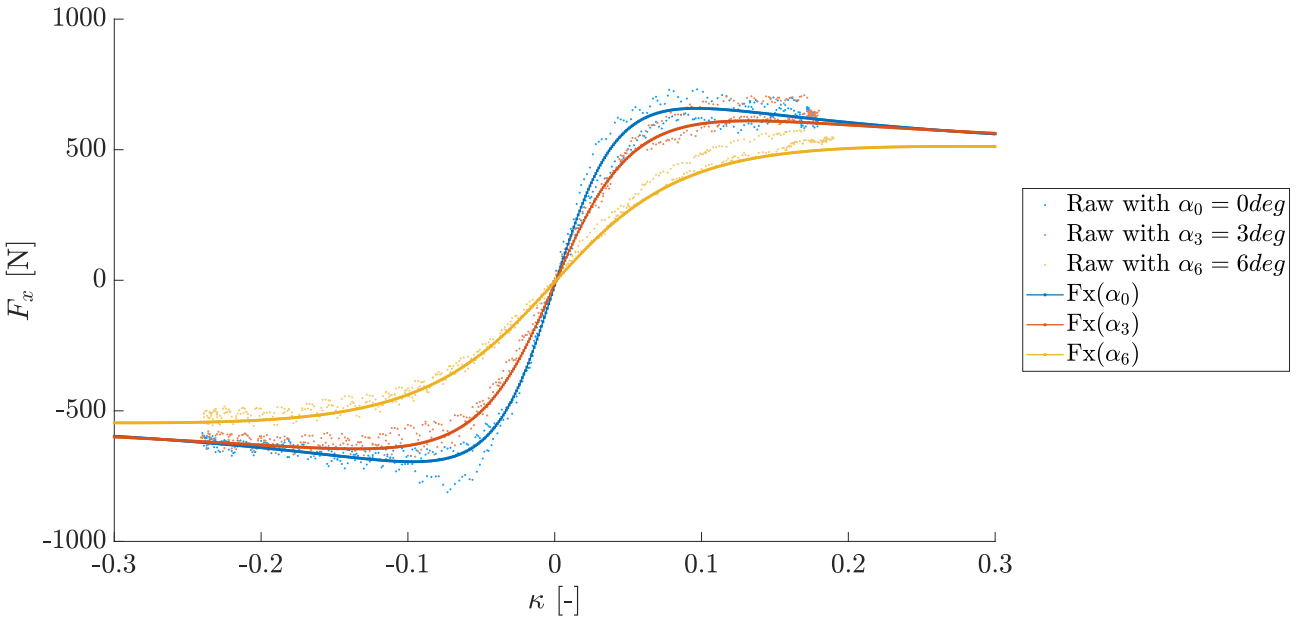


Figure 12: Comparison between the fitted curve on the raw data for the longitudinal force F_X as a function of κ for different side slip angles α .

To validate this result, it is important to calculate the weighting factor G_{xa} . The latter must always be greater than 0 and in pure conditions, that is, with $\alpha = 0$, as seen in the figure 13a, it must constant and equal 1.

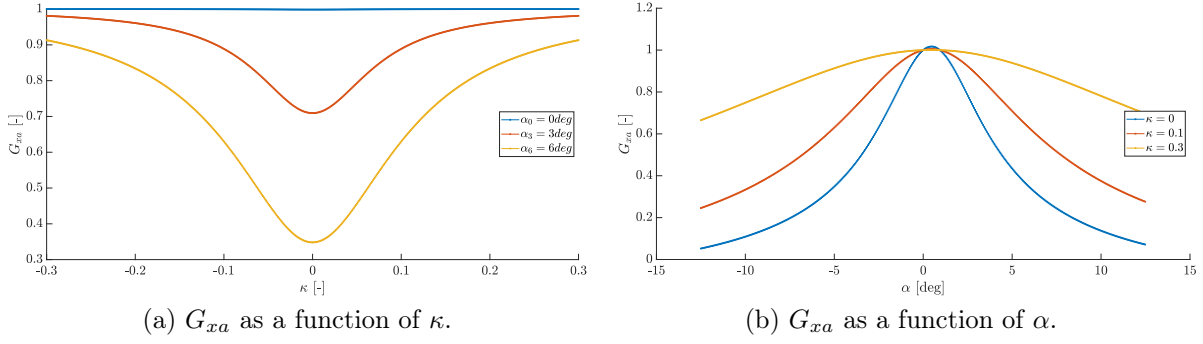


Figure 13: Plots of the weighting function G_{xa} of the longitudinal force F_X in combined behavior.

2.5 Combined lateral force

Again, the fitting is done using the variation of κ in the dataset in the range from -0.3 to 0.3 and varying the side slip angle α for the available three values: 0° , 3° and 6° . In the first analysis, the vertical load is kept equal to the nominal load F_{Z0} and the inclination angle is kept equal to 0 .

| | rBy1 | rBy2 | rBy3 | rCy1 | rHy1 | rVy1 | rVy4 | rVy5 | rVy6 |
|----------------------|---------------|---------|----------|-------|----------|-----------|---------|-------|---------|
| Guess | 7 | 2.5 | 0.1 | 1 | 0.02 | 0 | 30 | 1.9 | 10 |
| L bound | ~ | ~ | -3 | ~ | ~ | ~ | ~ | ~ | ~ |
| U bound | ~ | ~ | -3 | ~ | ~ | ~ | ~ | ~ | ~ |
| Optm par | 8.782 | 1.117e1 | 4.555e-3 | 1.223 | 9.987e-4 | -2.381e-2 | 1.677e1 | 1.082 | 5.084e1 |
| R² | 0.9921 | | | | | | | | |

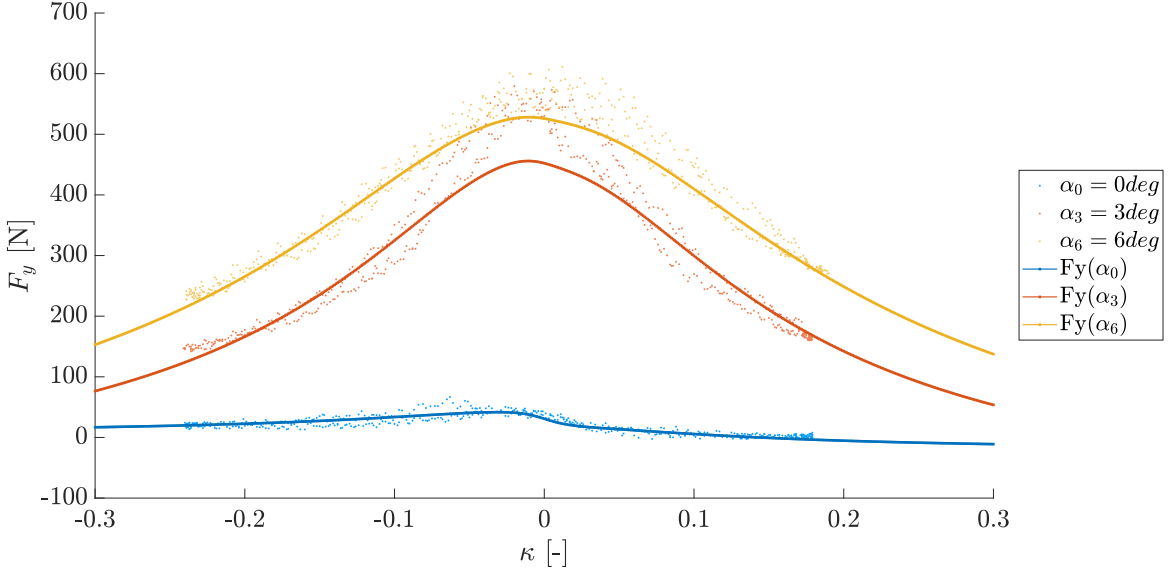


Figure 14: Comparison between the fitted curve on the raw data for the lateral force F_Y as a function of κ for different side slip angles α .

As in the longitudinal case, the weighting factor G_{ky} is calculated, which is useful to validate the result obtained.

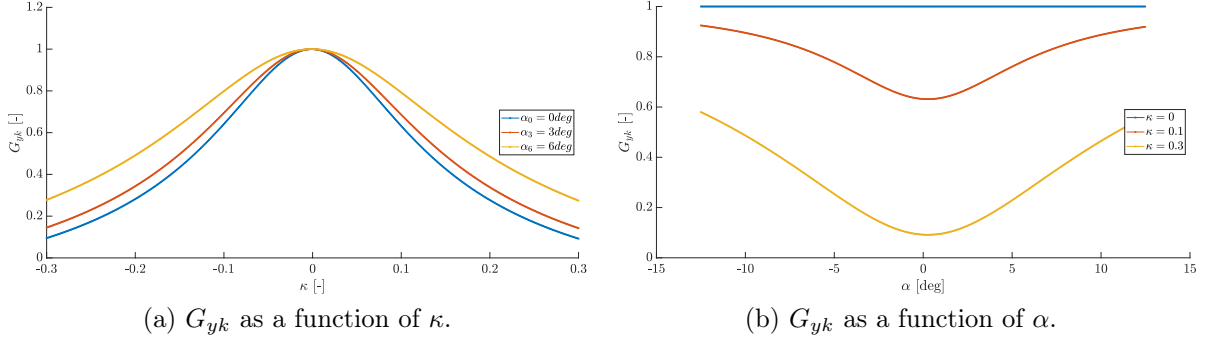


Figure 15: Plots of the weighting function G_{yk} of lateral force F_Y in combined behavior.

In addition, two additional optimizations, related to load and camber angle variation, respectively, were also included for lateral force. In this case, two parameters were optimized, one for each variation. The results obtained are not very accurate given the lack of enough data to be able to evaluate this variation, nevertheless, however, they have been reported.

| rVy2 | | rVy3 | |
|----------------------|---------------|----------------------|---------------|
| Guess | -0.01 | Guess | 1 |
| L bound | ~ | L bound | 0.7 |
| U bound | ~ | U bound | ~ |
| Optm par | -1.736e-2 | Optm par | 7e-1 |
| R² | 0.9709 | R² | 0.9848 |

The following graphs show the fitting for load change while maintaining a side slip angle equal to 6° and for camber change while maintaining $\alpha = 3^\circ$, respectively figure 16 and figure 17.

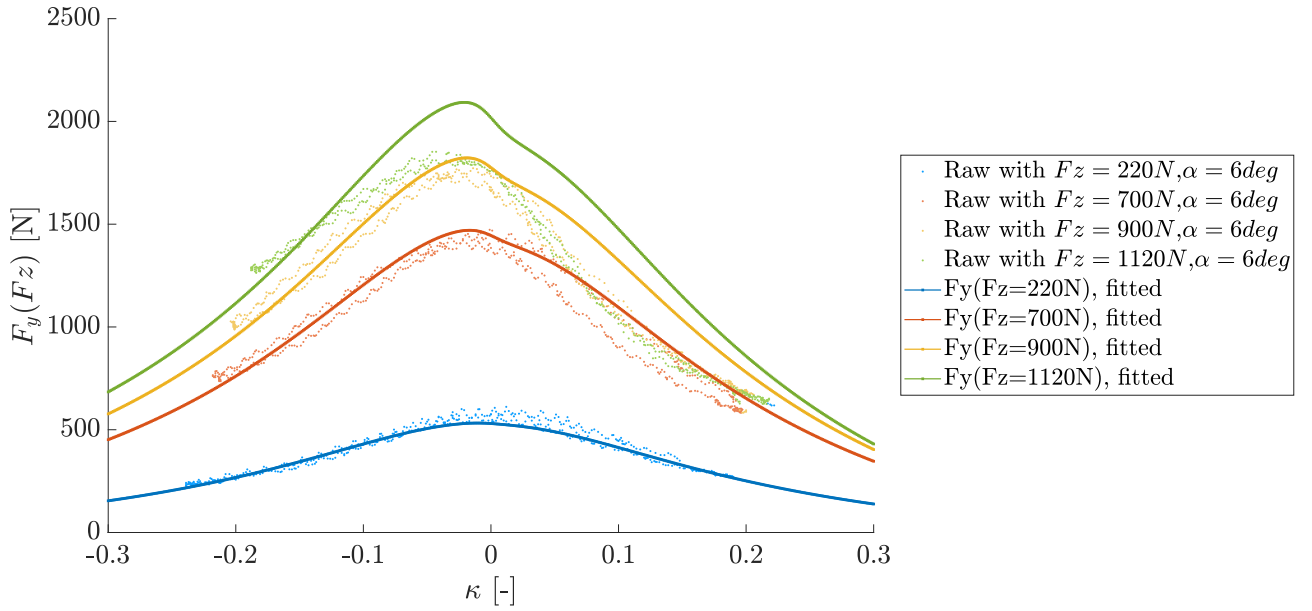


Figure 16: Comparison between the fitted curve on the raw data for the longitudinal force F_Y as a function of κ for $\alpha = 6^\circ$ and different vertical loads F_Z .

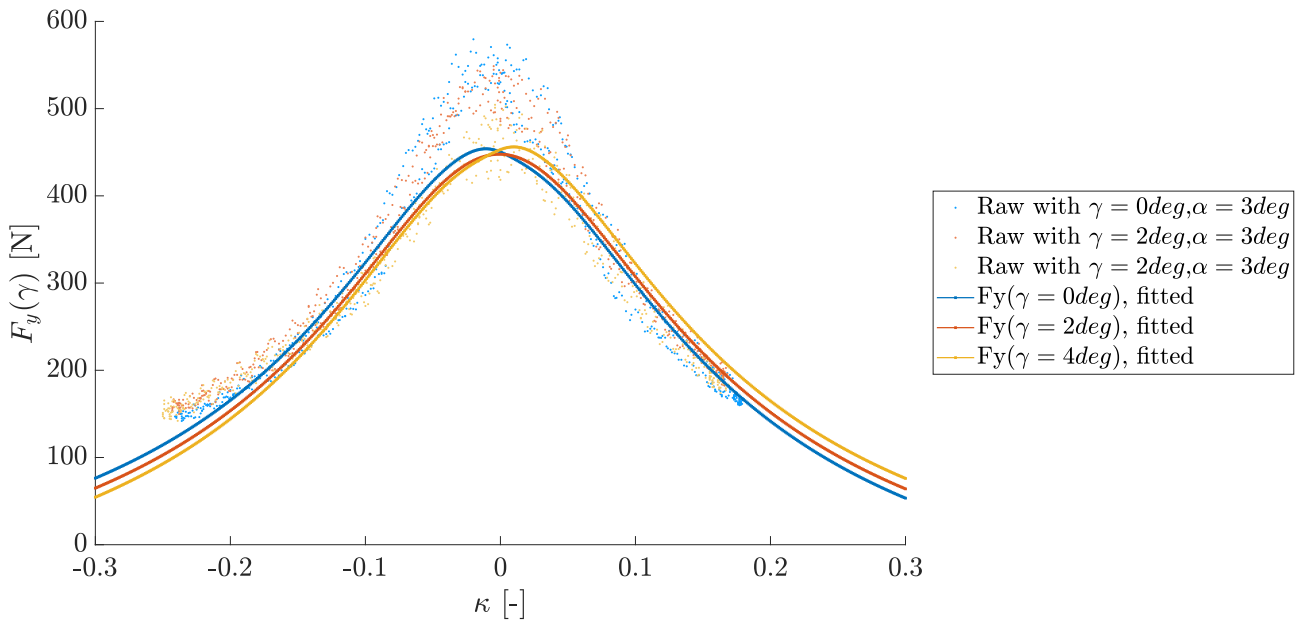


Figure 17: Comparison between the fitted curve on the raw data for the longitudinal force F_Y as a function of κ for $\alpha = 3^\circ$ and different camber angles γ .

3 Result discussion

In this chapter will be presented the principal and more significant steps that the team faced. The most difficult point has been the research of the initial guess to start the optimization. Even if, after finding them out with optimal curve fitting results, it has been discovered that it is not said that this is the best solution. It is important to underline that also the variations are determined under the influence of the reference curve fitted parameter: too much precise or strict parameters on the first one are able to fit very well the nominal curve but on the other hand can not fit correctly the varied curves in terms of load and camber.

This behavior has been discovered when team tries to better accommodate the fitting of the variation curves without being successful.

Sliders, within the live MATLAB script, were also used to carefully observe the effect of each parameter on the curve, the latter combined with theoretical observations, calculating the coefficients of the Magic Formula.

3.1 Cornering stiffness focus

The cornering stiffness behavior is essentially identified by its pick value, point p_1 in figure 18, and by its corresponding vertical force applied. In particular the parameters that are the responsible are the following:

$$p1 = F_{Z0} \cdot pKy1 \quad p2 = F_{Z0} \cdot pKy2 \quad (4)$$

with F_{Z0} denoting the nominal vertical wheel load [1].

A first result has been denoted by a non saturating behavior for the stiffness curve that presented a pick value p_1 lower than the previous, as shown in figures 19a and 20a. This error has been computed to a wrong initial guess of the pure lateral curve fitting, that it has been discovered to be the responsible of the combine and moment studies.

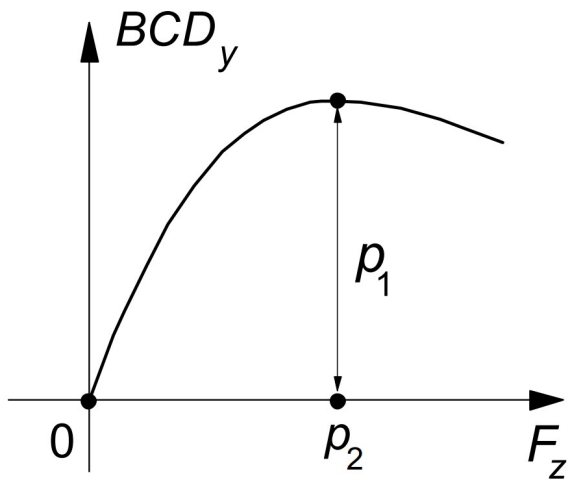
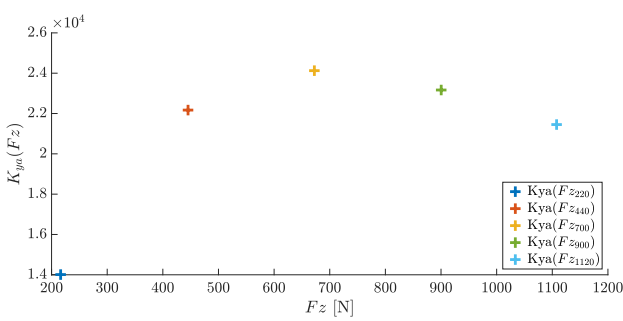


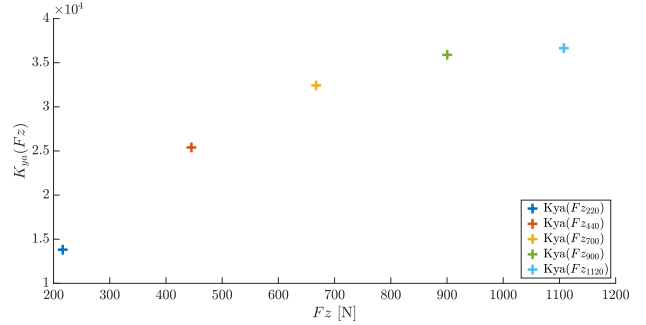
Figure 18: Cornering stiffness vs vertical load, from Hans Pacejka book *Tire and vehicle dynamics*.

Team 6 faced out these problems, being forced to recompute by scratch the entire guesses and boundaries limits, starting from the pure lateral force model that, as it has been ascertained, is

the responsible also of all the behavior of all the successive goodness of fitting of the subsequent curves. This problem has been faced when at the end of the entire tyre fitting assignment it has been decided to compute the graphs of the tyre stiffness for longitudinal and lateral. The issue popped out looking at the lateral one: varying the vertical load, the lateral stiffness did not show an, as expected, increasing trend of the pick value, not saturating correctly the stiffness curves.

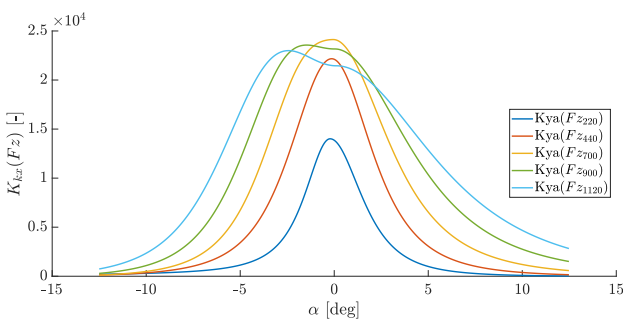


(a) K_{ya} obtained by old fitting parameters.

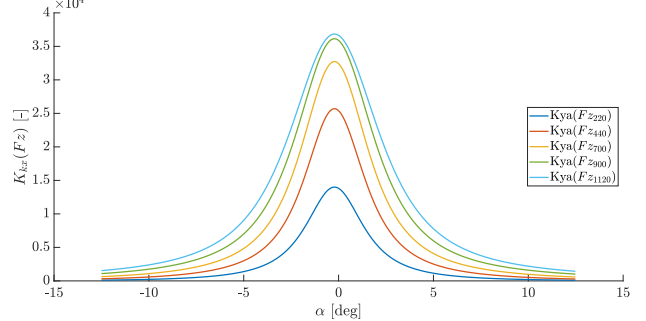


(b) K_{ya} obtained by new fitting parameters.

Figure 19: Comparison of plots of lateral cornering stiffness K_{ya} when the vertical load F_z changes.



(a) K_{ya} obtained by old fitting parameters.



(b) K_{ya} obtained by new fitting parameters.

Figure 20: Comparison of plots of lateral cornering stiffness K_{ya} in function of the side slip angle α .

3.2 Variable load on the pure lateral stiffness focus

Another point that saw a modification concerning the usage of new parameters and directly linked to the lateral cornering stiffness of chapter 3.1 is the variation load of the lateral force of paragraph 2.2.2. It has seen a little worsening behavior in terms of goodness of fitting. With the new compilation of the code with updated parameters, for all graphs with the last parameters version it has been noticed that the fitting does not match as good as the previous version. The result is any case not bad at all but the difference is evident in particular in the middle zone between the origin and the ceiling zone. This behavior can be seen looking at the following graphs developed using two different fitting parameters of the pure lateral forces.

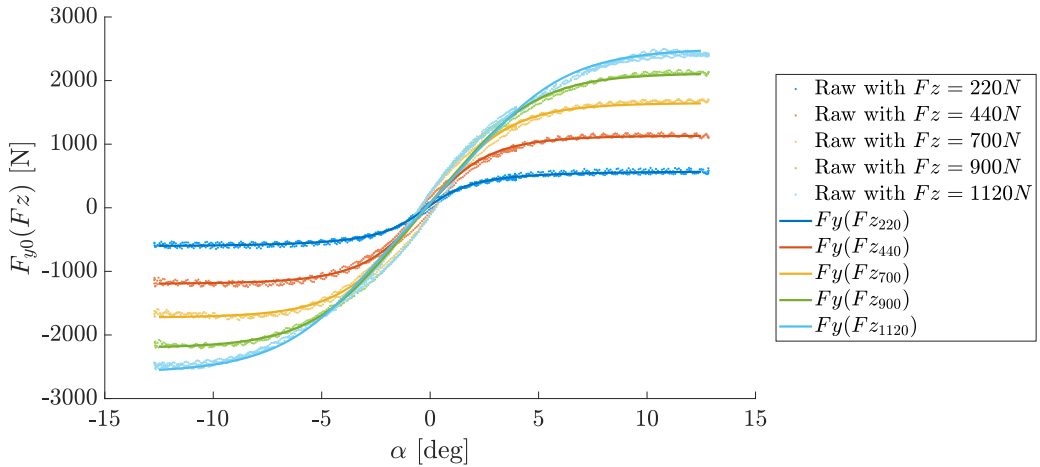


Figure 21: Fitted curve $F_{Y0}(F_Z)$ with old optimized parameters.

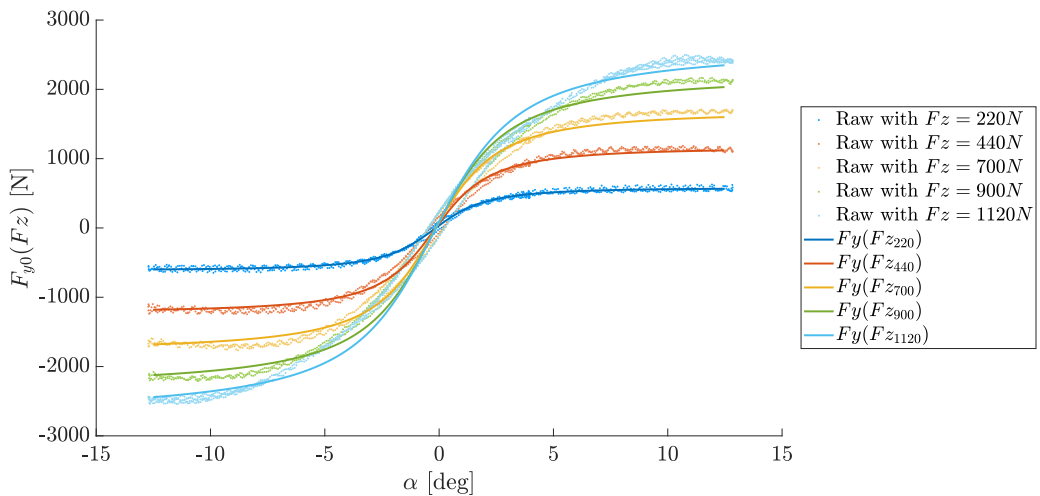


Figure 22: Fitted curve $F_{Y0}(F_Z)$ with new optimized parameters.

Few words about the valuation of the good of fitness of these two curves to support this thesis: the R^2 indices for both fitting procedures were recalculated: the former has an $R^2 = 0.9963$, while the latter has a lower $R^2 = 0.9912$.

Looking at the data, it can be seen that the slope of the trend of the points in the origin as the vertical load changes is not very different. That is why in an initial fitting procedure, using standard parameters and without imposing very stringent limits on $pKy1$ and $pKy2$, lateral cornering stiffness K_{ya} could not be obtained to saturate after the maximum load value imposed during the test. More stringent boundaries were imposed on the above parameters to achieve this behavior.

4 Conclusion

In conclusion, the coefficients implemented within the Magic Formula after the optimization procedures are reported. They are calculated in the worst conditions for each case.

| F_{X0} | F_{Y0} | M_{Z0} |
|-------------------|-------------------|----------------------|
| $B_x = 14.77$ | $B_y = 11.31$ | $B_r = -4.434$ |
| $C_x = 1.538$ | $C_y = 1.135$ | $B_t = 1.4916$ |
| $D_x = 2.167e3$ | $D_y = 2.567e3$ | $C_t = 4.999$ |
| $E_x = 0.2788$ | $E_y = 0.9474$ | $D_r = 48.14$ |
| $S_{Vx} = -213.4$ | $S_{Vy} = 47.99$ | $D_t = 0.041$ |
| $S_{Hx} = 0.0043$ | $S_{Hy} = 0.0038$ | $E_t = -0.1087$ |
| $\mu_x = 1.9347$ | $\mu_x = 2.3724$ | $\alpha_r = 0.0052$ |
| | | $\alpha_t = -0.0426$ |

With this assignment, Team 6 had the opportunity to understand the construction of a tyre model using the Magic formula 96 applied on two different type of dataset from a formula SAE tyre. The study started learning the in-class-provided files for the pure longitudinal force case. Then, making the the necessary changes to the code and creating the inherent functions, all has been re-adapted to the pure lateral forces, then for the aligning moment, and to conclude with the combined force behavior, both for longitudinal and lateral forces. A focus on the lateral and longitudinal stiffness has done in order to better understand if the fitting procedure has been done correctly. The report concludes with the tyre fitting parameter list that are the total output of this entire study.

References

- [1] Hans Pacejka. *Tire and vehicle dynamics*. Elsevier, 2005.